ZEBRAFISH GPR161 CONTRIBUTES TO BASAL HEDGEHOG REPRESSION IN A TISSUE-SPECIFIC MANNER

Philipp Tschaikner[1, 2], Dominik Regele[1], Willi Salvenmoser[3], Stephan Geley[4], Eduard Stefan[2], Pia Aanstad[1]

[1]Institute of Molecular Biology and Center for Molecular Biosciences, University of Innsbruck, Innsbruck, Austria

[2]Institute of Biochemistry and Center for Molecular Biosciences, University of Innsbruck, Innsbruck, Austria

[3]Institute of Zoology and Center of Molecular Bioscience Innsbruck, University of Innsbruck, Innsbruck, Austria

[4]Division of Molecular Pathophysiology, Medical University of Innsbruck, Innsbruck, Austria

*Corresponding author: Pia.Aanstad@uibk.ac.at

Abstract

Hedgehog (Hh) ligands act as morphogens to direct patterning and proliferation during embryonic development. Protein kinase A (PKA) is a central negative regulator of Hh signalling, and in the absence of Hh ligands, PKA activity prevents inappropriate expression of Hh target genes. The $G_{\alpha s}$-coupled receptor Gpr161 contributes to the basal Hh repression machinery by activating PKA, although the extent of this contribution is unclear. Here we show that loss of Gpr161 in zebrafish leads to constitutive activation of low-, but not high-level Hh target gene expression in the neural tube. In contrast, in the myotome, both high- and low-level Hh signalling is constitutively activated in the absence of Gpr161 function. Our results suggest that the relative contribution of Gpr161 to basal repression of Hh signalling is tissue-specific. Distinct combinations of G-protein-coupled receptors may allow the fine-tuning of PKA activity to ensure the appropriate sensitivity to Hh across different tissues.

Introduction

The Hh signalling pathway is a key regulator of cell fate specification and proliferation during embryonic development, and plays important roles in adult tissue homeostasis (Briscoe and Thérond, 2013; Ingham et al., 2011). Dysregulation of Hh signalling can lead to the formation of common and severe forms of human cancers such as basal cell carcinoma and medulloblastoma (Jiang and Hui, 2008; Raleigh and Reiter, 2019).

When Hh ligands bind their receptor Patched (Ptch), the inhibition of Smo by Ptch is alleviated, and Smo localises to the primary cilium (Corbit et al., 2005), where it activates downstream signalling to regulate the activity of the bifunctional Gli transcription factors.

Hh ligands act as morphogens, and the transcriptional outcome of Hh signalling is determined by the balance between repressor and activator forms of the Gli transcription factors. This balance is controlled by the activity of PKA and other kinases (Hui and Angers, 2011; Niewiadomski et al., 2019). In the absence of Hh, the basal Hh repression machinery is thought to maintain a high level of PKA activity. PKA phosphorylates the Gli proteins and primes them for further phosphorylation and proteolytic cleavage, to yield truncated forms that act as transcriptional repressors (GliR) (Niewiadomski et al., 2014; Pan et al., 2009; Wang et al., 2000). In addition, PKA also plays a role in restricting the activity of full length Gli (GliA) by promoting its association with Sufu (Humke et al., 2010; Marks and Kalderon, 2011). Low levels of exposure to Hh ligands blocks the formation of GliR, whereas high levels of Hh exposure is required for the formation of the activator forms of Gli. This is thought to be controlled through a cluster of six PKA target residues in Gli, with distinct phosphorylation patterns regulating the formation of repressor and activator forms (Niewiadomski et al., 2014). This rheostat mechanism ensures that the level of Gli transcriptional activity corresponds to the level of PKA activity, which in turn must be controlled by the level of Smo activity and Hh ligand exposure (Niewiadomski et al., 2019, 2014). Consistent with this, a complete loss of PKA activity leads to constitutive (Smo-independent) maximal Hh signalling, whereas constitutive activation of PKA abolishes all Hh-dependent transcription (Hammerschmidt et al., 1996; Tuson et al., 2011; Zhao et al., 2016).

A central and long-standing question in Hh signalling regards the nature and regulation of the basal repression machinery and the mechanism of regulation. In *Drosophila,* Smo has been shown to regulate PKA activity directly by activating $G_{\alpha i}$-proteins to modulate cAMP levels (Ogden et al., 2008). Although vertebrate Smo can also couple to $G_{\alpha i}$ (Riobo et al., 2006), it is clear that $G_{\alpha i}$ is not required for all aspects of vertebrate Hh signalling (Ayers and Thérond, 2010), raising the question which other mechanisms contribute to the regulation of PKA.

The murine orphan G-protein coupled receptor (GPCR) Gpr161 contributes to basal Hh repression by activating $G_{\alpha s}$ and consequently PKA (Mukhopadhyay et al., 2013). In the absence of Hh ligands, Gpr161 localises to the primary cilia, and is removed from the cilia upon activation of Smo (Mukhopadhyay et al., 2013; Pal et al., 2016). These results suggest that Gpr161 maintains PKA activity in the cilium in the absence of Hh, and that the ciliary exit of Gpr161 is required for Hh signalling and the reduction of PKA activity (Mukhopadhyay et al., 2013; Pal et al., 2016). However, Gpr161 has also been shown to be a substrate of PKA, and can act as an A kinase anchoring protein (Bachmann et al., 2016; Torres-Quesada et al., 2017). Thus, the exact molecular mechanisms that regulate Gpr161 activity in the context of Hh signalling remain unclear.

Gpr161 mutants display severe developmental malformations, including craniofacial defects and ventralisation of the neural tube, that were independent of Smo function, suggesting that Gpr161 causes constitutive activation of downstream Hh signal transduction (Mukhopadhyay et al., 2013). However, the neural tube of Gpr161 mutants was less severely ventralised than that observed in embryos completely lacking PKA activity (Tuson et al., 2011). In neural progenitor cells (NPCs), Gpr161 was found to be epistatic to Smo only for low level signalling, while expression of high level targets such as Nkx2.2 and FoxA2 still depended on Smo function (Pusapati et al., 2018), suggesting that in the neural tube, Gpr161 plays an important role in controlling basal and low level Hh signalling activity. In murine NIH 3T3 fibroblasts, loss of Gpr161 does not affect basal repression, although the mutant cells displayed an increased sensitivity to Hh ligands. Taken together, these results suggest that additional $G_{\alpha s}$-coupled receptors may be involved in maintaining PKA activity in the absence of Hh ligands (Pusapati et al., 2018). Supporting this, several studies have identified additional GPCRs that regulate Hh signalling in parallel or downstream of Smo (Klein et al., 2001; Singh et al., 2015; Stückemann et al., 2012).

To facilitate the study of Gpr161 in Hh signalling during development, we have generated zebrafish *gpr161* mutants, and show that Gpr161 is an important negative modulator of Hh signalling in zebrafish embryos. We find that in the zebrafish neural tube, Gpr161 is epistatic to Smo for low-level Hh targets, however the activation of high-level targets depends on Smo activity in *gpr161* mutants. Interestingly, in the myotome, both high and low levels of Hh signalling are independent of Smo function, suggesting that several GPCRs may be involved in regulating PKA activity during Hh signalling, and that the level of contribution of Gpr161 to basal repression of Hh signalling is tissue-specific.

Results

Gpr161 is an evolutionary conserved GPCR with two paralogs in zebrafish

The zebrafish genome contains two conserved paralogs of Gpr161, Gpr161a and Gpr161b, with 71% sequence identity and 84% sequence similarity between each other, and more than 70% similarity to the murine Gpr161 protein (Figure 1A, Figure 1 Supplement 1). Expression analysis using qRT-PCR showed that both transcripts are expressed during embryonic development, but while *gpr161b* is maternally provided, *gpr161a* expression is first detected at 9 hours post fertilisation (hpf) (Figure 1B). In mouse, Gpr161 localises to primary cilia, and this localisation has been proposed to be important for its role in modulating the Hh signalling pathway (Mukhopadhyay et al., 2013; Pal et al., 2016; Shimada et al., 2018). To test whether zebrafish Gpr161 also localise to primary cilia, we injected mRNA of Myc-tagged versions of Gpr161a and Gpr161b into one-cell stage zebrafish embryos. Both Gpr161a and Gpr161b were readily detected at primary cilia in gastrula stage zebrafish embryos (Figure 1C).

Gpr161a and Gpr161b are functionally redundant but essential during zebrafish embryonic development

To investigate the functional roles of Gpr161a and Gpr161b during zebrafish development, we used CRISPR/cas9 to generate mutant alleles for each gene, *gpr161a*^{ml200}, which carries a 6bp insertion in the second coding exon of *gpr161a,* and *gpr161b*^{ml201}*,* harboring an 8bp deletion in the second coding exon of *gpr161b*. Both alleles introduce premature stop codons within the 7-transmembrane-domain region of the respective proteins, and are predicted to be functionally inactive (Figure 1 Supplement 2). Animals homozygous for either *gpr161a*^{ml200} or *gpr161b*^{ml201} alone, or animals lacking three of the four *gpr161* alleles, showed no effect either on embryonic development or in adult viability and fertility. In contrast, *gpr161a; gpr161b* double zygotic homozygous mutant embryos showed clear morphological phenotypes by 24 hpf, suggesting that Gpr161a and Gpr161b act in a functionally redundant manner (Figure 2A). To determine the contribution of maternal Gpr161b, we generated embryos from incrosses of *gpr161b*$^{-/-}$*; gpr161a*$^{+/-}$ animals. Quantitative analysis of *gpr161a* expression at the 2 cell stage of these *MZgpr161b; gpr161a* mutant embryos showed that a complete loss of Gpr161b did not result in a compensatory maternal upregulation of Gpr161a (Figure 2 Supplement 1). We conclude that *MZgpr161b*$^{-/-}$*; gpr161a*$^{-/-}$ mutant embryos are likely to represent a complete loss of function of zebrafish Gpr161, and refer to these mutants as *gpr161* mutants below.

At 24hpf, *gpr161* mutant embryos display several developmental abnormalities, including malformed eyes lacking any obvious lens or retinal structure (Figure 2A). At this stage of development, wildtype embryos display chevron shaped somites, while the somites of *gpr161* mutants have a more obtuse angle (Figure 2A). These phenotypes, which are only present in the double mutant line, but not in

MZ*gpr161b*$^{-/-}$*; gpr161a*$^{+/-}$ or *gpr161b*$^{+/-}$*; gpr161a*$^{-/-}$ embryos, are similar to those observed in *ptch1*$^{-/-}$*; ptch2*$^{-/-}$ double mutant embryos (Koudijs et al., 2008). In contrast to *ptch1*$^{-/-}$*; ptch2*$^{-/-}$ double mutant embryos which lack eyes (Koudijs et al., 2008), a rudimentary eye can be identified in *gpr161* mutants at 72 hpf (Figure 2B).

At this stage, the retina of wild type embryos is organised into six evolutionarily conserved layers: the pigmented epithelium, the photoreceptor cell layer, the outer plexiform layer, the inner nuclear layer, the inner plexiform layer, and the ganglion cell layer (Schmitt and Dowling, 1999). Semi-thin sectioning revealed that while eye morphogenesis was abnormal, remnants of all six layers were clearly identified by morphology (Figure 2D, Figure 2 Supplement 2A). However, these layers are not well separated and the optic cup is partially folded (Figure 2 Supplement 2B). Additionally, remnants of a forming lens can be found in *gpr161* mutant embryos (Figure 2 Supplement 2A). A striking phenotype of the *gpr161* mutants is the complete loss of jaw structures (Figure 2B), as demonstrated by scanning electron microscopy (SEM) imaging, which revealed that *gpr161* mutant embryos display an open pharynx with a complete lack of all jaw structures (Figure 2C). While *ptch1*$^{-/-}$*; ptch2*$^{-/-}$ double mutant embryos were reported to lack all olfactory structures (Koudijs et al., 2008), SEM imaging revealed that in the *gpr161* mutants the olfactory pits are present, though severely reduced in size (Figure 2C).

Zebrafish embryos with a strong Hh gain-of-function phenotype, such as the *ptch1*$^{-/-}$*; ptch2*$^{-/-}$ double mutants, also display defects in the development of the otic vesicles (Koudijs et al., 2008). The *gpr161* mutant embryos exhibited smaller otic vesicles compared to wild type embryos (Figure 2B). Serial sections of the otic vesicles revealed the absence of the dorsolateral septum (Figure 2 Supplement 2C). The combination of developmental defects in ocular and otic structures is commonly seen in mutants of negative regulators of Hh signalling, such as *sufu*, *ptch1* and *hhip* (Whitfield et al., 1996), and suggests that Gpr161 acts to negatively regulate Hh signalling also in zebrafish.

Gpr161 mutant mice do not form limb buds (Hwang et al., 2018; Mukhopadhyay et al., 2013) and *ptch1*$^{-/-}$*; ptch2*$^{-/-}$ double mutant zebrafish embryos lack pectoral fin buds (Koudijs et al., 2008). In contrast to the requirement for Gpr161 in murine limb formation, pectoral fin formation appeared normal in the zebrafish *gpr161* mutant embryos. (Figure 2B, Figure 2 Supplement 2D).

Hedgehog signalling is upregulated in *gpr161* mutant embryos

The morphological phenotypes observed in *gpr161* mutants are consistent with increased Hh signalling. To determine whether Hh signalling is upregulated in *gpr161* mutants, we assessed the expression of known Hh target genes in the neural tube by qRT-PCR and RNA *in situ* hybridisation. The Hh target genes *ptch2, gli1, nkx2.2b* and *nkx6.1* (Figure 3B) were all strongly upregulated, while

158 *pax7a,* which is repressed by Hh signalling (Guner and Karlstrom, 2007), was strongly downregulated
159 in *gpr161* mutant compared to wild type embryos (Figure 3B). RNA in situ hybridisation revealed that
160 expression of *shha,* the major Hh ligand expressed in the neural plate was not expanded in *gpr161*
161 mutants (Figure 3A). However, expression of *ptch2*, a direct transcriptional target of Hh signalling
162 (Concordet et al., 1996), was expanded in *gpr161* mutants (Figure 3A), suggesting that Hh signalling is
163 upregulated in *gpr161* mutants downstream of Shh expression. Similarly, expression of *olig2,* a
164 marker of motor neuron induction which depends on low-level Hh activity (Dessaud et al., 2007; Park
165 et al., 2002), as well as *nkx2.2a,* a marker for V3 interneuron progenitor cells of the lateral floorplate
166 (Barth and Wilson, 1995; Briscoe et al., 1999), were clearly expanded in the *gpr161* mutant neural
167 tube (Figure 3A). We note that the expansion of the low-level target *olig2* appears to be stronger
168 than the expansion of the high-level target *nkx2.2a* (Figure 3A). Taken together, these results show
169 that loss of Gpr161 leads to a hyperactivation of the Hh signalling pathway in zebrafish.

170 In the zebrafish myotome, sustained Hh signalling during gastrulation and somitogenesis stages have
171 been shown to be required for the specification of several cell types, including Prox1 and Eng double
172 positive muscle pioneer cells (MPs) and Prox1 positive superficial slow fibres (SSFs) (Wolff et al.,
173 2003). While medium-to-low level Hh signalling is sufficient for the specification of SSFs, the
174 formation of MPs requires high levels of Hh (Wolff et al., 2003). Consistent with the expansion of Hh
175 target genes in the neural tube, *gpr161* mutants also displayed an increase in both SSFs and MPs
176 (Figure 3C). While zygotic Gpr161 loss of function resulted in a significant increase in both SSFs (from
177 22 ± 2 (mean ±SD) in wt to 33 ±5 in zygotic *gpr161* mutants) and MPs (from 4 ± 1 (mean ± SD) in wt
178 to 7 ± 2 in zygotic *gpr161* mutants), complete loss of both maternal and zygotic Gpr161 led to a
179 stronger increase in both SSFs and MPs (56 ± 9 (mean ± s.d.) SSFs, and 23 ± 10 MPs), consistent with
180 the requirement for sustained Hh signalling in muscle cell development (Wolff et al., 2003). These
181 results suggest that in the somites, loss of Gpr161 results in expansion of both high and low Hh
182 signalling targets.

183 ## *gpr161* mutants remain sensitive to Shh

184 Our results suggest that although loss of Gpr161 function in zebrafish leads to increased Hh signalling
185 activity, *gpr161* mutants display weaker phenotypes than those seen in mutants with maximal
186 activation of Hh signalling. To determine whether Hh signalling could be further activated in *gpr161*
187 mutants in response to Hh, we injected 50 or 100 pg *shh* mRNA, and assessed SSF and MP formation
188 using Prox1 and Eng antibody staining as above (Figure 4A-B). In wild-type embryos, overexpression
189 of 100 pg *shh* resulted in an approximate 1.8-fold increase in both MPs and SSFs (Figure 4B), a
190 significant change from uninjected control embryos (ANOVA, SSFs $p<0.01$, MPs $p<0.01$). In contrast,
191 neither 50 nor 100 pg *shh* resulted in a significant increase in the number of SSFs in *gpr161* mutant

embryos (ANOVA, 50 pg p>0.9, 100 pg p>0.5), suggesting that the number of SSFs have reached a maximum level in the uninjected mutants. Injection of 100 pg *shh* did, however, give a significant 1.9-fold increase in the number of MPs in *gpr161* mutant embryos (ANOVA, p<0.001) (Figure 4B). Taken together, these results suggest that in the *gpr161* mutant, medium-to-low level Hh signalling targets are activated close to maximal levels, whereas high level targets of Hh signalling are increased, but not maximally so.

Activation of PKA rescues *gpr161* mutant phenotypes

Murine Gpr161 was proposed to act as a constitutively active $G_{\alpha s}$-coupled receptor, which contributes to maintain basal levels of PKA activity to keep the Hh pathway inactive (Mukhopadhyay et al., 2013). This model predicts that the phenotypes observed in the *gpr161* mutants are due to a loss of adenylate cyclase activity, and should be rescued by artificial activation of adenylate cyclase by agents such as forskolin. Previous studies have reported that 300 µM forskolin phenocopies a complete loss of Hh signalling (Barresi et al., 2000). Consistent with this, treatment with 300 µM forskolin resulted in a near complete loss of all MPs and SSFs in wild-type as well as *gpr161* mutant embryos (Figure 5A-B), consistent with the model that hyperactivation of Hh signalling in the *gpr161* mutants is due to a reduction of PKA activity. Treatment with lower concentrations of forskolin, ranging from 500 nM to 50 µM, had only minor effects on somite development of wild-type embryos, but resulted in a significant degree of rescue of the *gpr161* mutant phenotype (Figure 5A-B). We note that MPs, which require high levels of Hh signalling, were more sensitive to forskolin concentrations than SSFs, which require low levels of Hh.

Distinct contributions of Gpr161 to basal repression of Hh signalling in different tissues

To determine the epistatic relationship between Smo and Gpr161 in zebrafish, we used the zebrafish *smo* null allele *hi1640* (Chen et al., 2001) to generate zebrafish *gpr161b*$^{-/-}$*; gpr161a*$^{-/-}$*; smo*$^{-/-}$ triple mutants, and assessed Hh signalling activity using Prox1/Eng staining and neural tube markers, as above. Zebrafish *gpr161b*$^{-/-}$*; gpr161a*$^{-/-}$*; smo*$^{-/-}$ triple homozygous mutant embryos showed a morphological phenotype, as well as an expansion of both SSFs and MPs, that were indistinguishable from *gpr161b*$^{-/-}$*; gpr161a*$^{-/-}$ double homozygous mutant embryos (Figure 6A-B, Figure 6 Supplement 1), consistent with the reported phenotypes in the mouse *Gpr161*;*Smo* double mutants (Mukhopadhyay et al., 2013). Further, the expansion of low-level Hh target-genes *ptch2* and *olig2* was similarly found to be independent of Smo function (Figure 6C). In contrast, the double mutant *gpr161*$^{-/-}$*; gpr161a*$^{-/-}$*; smo*$^{-/-}$ triple mutant embryos showed no detectable *nkx2.2a* expression, suggesting that in the neural tube, though not in the somites, high level Hh target gene expression is dependent on Smo function in the absence of Gpr161.

Discussion

Hh signalling is tightly controlled at multiple levels in order to accurately translate morphogen gradients into graded transcriptional responses mediated by the Gli transcription factors. PKA both promotes formation of the Gli repressor forms and inhibits Gli activator forms, thereby controlling sensitivity to Hh ligands, and providing a filter for Hh signalling strength. How PKA activity is fine-tuned in Hh signalling is not completely understood. GPCRs such as Gpr161 have been shown to impact on Hh signalling by regulating PKA via the regulation of adenylate cyclase activity. To extend our understanding of how GPCRs regulate Hh signalling, we generated zebrafish *gpr161* mutants and analysed Hh-dependent signalling in the neural tube and the myotome.

The zebrafish genome contains two conserved Gpr161 orthologues, Gpr161a and Gpr161b. We have generated mutants for both orthologues, and show that Gpr161a and Gpr161b act redundantly in early zebrafish development. Zebrafish mutants lacking Gpr161 function show an expansion of Hh target gene expression both in the neural tube and in the somites, and develop severe craniofacial defects that are similar to those described for the *ptc1*$^{-/-}$*; ptc2*$^{-/-}$ double mutants (Koudijs et al., 2008). These results confirm that the role of Gpr161 as a modulator of Hh signalling is conserved in the vertebrate lineage.

Gpr161 was proposed to contribute to the basal Hh repression machinery by activating $G_{\alpha s}$ and adenylate cyclase, resulting in activation of PKA, and overexpression of murine Gpr161 was shown to lead to a general increase in intracellular cAMP levels (Mukhopadhyay et al., 2013). However, direct evidence for reduced cAMP production in Gpr161 mutant cells is hampered by the difficulties in measuring physiological cAMP levels in specific subcellular compartments such as the primary cilium. We have taken advantage of the zebrafish embryo's amenability to pharmacological treatments to further probe the mechanism of Gpr161 action. Consistent with the model that loss of Gpr161 leads to lowered cAMP levels and reduced PKA activity, we found that treatment with the cAMP elevating agent forskolin fully rescued muscle cell specification in the *gpr161* mutant embryos. Interestingly, a 100-fold concentration range (0.5-50 µM) of forskolin gave very similar near-complete rescue of both mutant morphology and molecular read-outs of both high and low level Hh target gene expression in the somites, suggesting that additional mechanisms may be in place to ensure appropriate regulation of PKA activity in the presence of excess cAMP. Previous studies have reported that loss of Gpr161 may also affect other signalling pathways in addition to Hh signalling (Li et al., 2015; Mukhopadhyay et al., 2013). While we cannot rule out a role for Gpr161 in processes not related to Hh signalling, our results suggest that loss of Gpr161 function can be fully compensated by artificial activation of adenylate cyclase.

A comparison of phenotypes suggests that the upregulation of Hh signalling in zebrafish *gpr161* mutants is less severe than that seen in *ptc1*$^{-/-}$*; ptc2*$^{-/-}$ mutant embryos (Koudijs et al., 2005). Similarly, injection of a dominant-negative form of PKA resulted in an apparently stronger increase in Hh-dependent muscle cell specification in the myotome than could observed in the *gpr161* mutants (Zhao et al., 2016). This is consistent with data obtained in mice, where a loss of PKA or $G_{\alpha s}$ leads to more severe ventralisation of the neural tube than what is observed in the *Gpr161* mutants (Mukhopadhyay et al., 2013; Pusapati et al., 2018; Regard et al., 2013; Tuson et al., 2011). Further supporting the idea that Hh signalling is not maximally activated in the *gpr161* mutants, we find that injection of *shha* mRNA can further increase high, but not low, level Hh targets in the somites of *gpr161* mutants. Thus we conclude that whereas low level Hh signalling is maximally active in the *gpr161* mutants, additional mechanisms contribute to PKA activation to control high level Hh signalling in the absence of Gpr161 function.

Importantly, we also show that low level Hh signalling in the neural tube of *gpr161* mutants is independent of Smo, whereas expression of the high level Hh target gene *nkx2.2a* clearly requires Smo function. Our results are consistent with the model that $G_{\alpha s}$-coupling and activation by Gpr161 is one of several mechanisms that contribute to the mobilisation of compartmentalised cAMP to repress Hh target activation, and that the reduction in cAMP levels caused by loss of Gpr161 is sufficient to cause constitutive, Smo-independent activation of low, but not high level Hh signalling. This result provides genetic evidence to support the model based on results from pharmacological inhibition of Smo in mammalian cell culture (Pusapati et al., 2018). Similar experiments were performed in the mouse *Gpr161* mutant, with the conclusion that Gpr161 is largely epistatic to Smo (Mukhopadhyay et al., 2013). These authors do however note that the expression of high level Hh target genes, such as Nkx2.2 and FoxA2, is reduced in *Smo; Gpr161* double mutants compared to *Gpr161* single mutants. One possibility is that this difference is due to the different assays used to assess Hh target gene expression in mouse and zebrafish neural tubes. Whereas Mukhopadhyay and colleagues used immunohistochemistry to detect Hh target gene expression (Mukhopadhyay et al., 2013), our results are based on chromogenic in situ hybridisation, a far less sensitive assay. Thus, we can not rule out that some low level *nkx2.2a* expression persists in the zebrafish triple mutants. Another possibility is that there could be species-specific differences in the roles of GliR and GliA and/or cAMP levels, or alternatively, Gpr161 may make a relatively larger contribution to cAMP levels in the zebrafish neural tube compared to mouse. Interestingly, we do observe tissue-specific differences in zebrafish in our epistasis experiments. In the *gpr161* mutant myotome, both high and low level Hh signalling outcomes are independent of Smo, suggesting that in the somites Gpr161 is completely epistatic to Smo. We suggest that in the neural tube, additional unknown factors make significant contributions to promote basal cAMP levels, whereas in the zebrafish myotome, Gpr161

alone may account for the largest part of the basal repression machinery. Thus, distinct combinations of GPCRs in different cell types can contribute to complex and tissue-specific regulation of Hh signalling. The identification of these additional GPCRs, as well as other factors that control PKA activity downstream of adenylate cyclases, will be required to understand how Hh signalling is fine-tuned to orchestrate the great variety of Hh-dependent biological processes in a cell type specific manner.

Materials and Methods

CRISPR/cas9 genome editing and genotyping

Guide RNAs for CRISPR/cas9 mediated knockout of both *gpr161a* (ENSDART00000151311.2) and *gpr161b* (ENSDART00000078051.6) were designed using the ChopChop web tool (Montague et al., 2014) and synthesised as described previously (Huang et al., 2014). Embryos were injected with 50 pg of gene specific sgRNA and 300pg of *cas9* mRNA at 1-cell stage. F0 founder fish were identified by T7 Endonuclease I digests of gene-specific PCR products from pooled genomic DNA obtained from F1 offspring, following the manufacturer's protocol (NEB, #M0302L). While the *gpr161a*^{ml200} allele harbors an 8bp deletion, the introduced mutation in *gpr161*^{ml201} leads to a 6bp insertion, which were identified by running out gene specific PCR products (see Table 2) on 4% agarose gels. Genotyping of the *smo*^{hi1640} allele was performed as described previously (Chung and Stainier, 2008).

Zebrafish lines and husbandry

All zebrafish lines including SAT wildtype strains were kept at 28°C according to standard protocols.

MZ*gpr161b*$^{-/-}$; *gpr161a*$^{-/-}$ embryos were obtained by performing in-crosses of a *gpr161b*$^{-/-}$*; gpr161a* $^{+/-}$ line. Embryos were raised at 28°C and staged by morphology (Kimmel et al., 1995).

All experimental protocols concerning zebrafish were approved by the Austrian Ministry for Science and Research (BMWFW-66.008/0016-WF/V/3b/2016, BMBWF-66.008/0015-V/3b/2018), and experiments were carried out in accordance with approved guidelines.

Construction of plasmids

To generate expression-vectors for *gpr161a* and *gpr161b* the coding sequence of both genes were amplified with overlapping primers (see Table 2) using homemade PfuX7 polymerase (Nørholm, 2010) and fused in-frame to a Myc-Tag into pCS2+ by *in vivo* Assembly (IVA) cloning (García-Nafría et al., 2016).

Quantitative (q) RT-PCR

RNA was isolated from zebrafish embryos with Trizol (Ambion) following the manufacturer's instructions. RNA integrity was checked by agarose gel electrophoresis and the concentration was measured using a Nanodrop 2000c (Thermo) spectrophotometer.

Complementary DNA was transcribed from equal amounts of dsDNase-treated total RNA using the Maxima RT kit for qPCR (Thermo) with dsDNase according to the manufacturer's instructions.

RT-qPCRs were performed using 5x HOT FIREPol EvaGreen qPCR Supermix (Solis Biodyne) and contained each primer at 250nM and cDNA corresponding to a total RNA amount of 15 ng for pooled embryos or 5 ng for single embryos. PCRs were run on a CFX96 Connect (BioRad) under following conditions: 12 min 95°C, 40 cycles of 95°C for 30s, 60°C for 30s and 72°C for 20s. Melt curves were recorded from 65°C to 95°C in 0.5°C increments. Data was acquired using CFX Manager 3.1 (BioRad) and exported as RDML files for processing.

Data analysis was performed in R version 3.4.4. Fluorescence data were imported using the package RDML (Rödiger et al., 2017) and amplification curves fitted using the 'cm3' model (Carr and Moore, 2012) implemented in the package qpcR (Ritz and Spiess, 2008). The first derivative (d0) of the model was used as expression value. Expression values for genes of interest were normalised using the geometric mean of the expression values of the reference genes *eef1aa* and *rpl13*.

Whole-mount in situ hybridisation

In situ hybridisation was performed following standard protocols. DIG-labelled antisense probes were made for *shha* (Krauss et al., 1993), *ptch2* (Concordet et al., 1996), *olig2* (Park et al., 2002) and *nkx2.2a* (Barth and Wilson, 1995).

Immunohistochemistry

Embryos were fixed in 4% paraformaldehyde at room temperature for 3h, then washed in PBS-Triton (PBS + 0.3% Triton X-100). After 1h of incubation in blocking solution (PBS-Triton, 4% BSA, 0.02% NaN_3) at 4°C, primary antibodies diluted in blocking solution were added and left over night for incubation at 4°C. After subsequent washes in PBS-Triton embryos were incubated with appropriate Alexa conjugated secondary antibodies over night at 4°C. Again, Embryos were washed several times in PBS-Triton and mounted in Mowiol embedding medium for imaging. For a list of the antibodies used in this study, see Supplementary Table 1. All stainings were imaged using a Zeiss Axio Observer.Z1 microscope equipped with a Yokogawa CSU-X1 spinning disc confocal unit using 25x, or 63x water-immersion lenses.

Chemical treatments

For chemical treatments embryos were dechorionated at 50% epiboly and transferred to agar-coated 35mm dishes containing forskolin (Biomol) at final concentrations between 0.5 and 300 µM in 1% DMSO. Control experiments were performed simultaneously in 1% DMSO. All embryos were treated until 24 hpf.

Microinjection

mRNA was synthesised using the HiScribe SP6 RNA Synthesis Kit (NEB) and capped using the Vaccinia Capping System (NEB) following the protocols provided by the manufacturer. Embryos were injected at one-cell stage. Injected volumes are indicated in the respective figures.

Light Histology

Three day old (72 hpf) wild type and *gpr161* mutant embryos were fixed in 2.5% glutaraldehyde in 0.01M sodium cacodylate buffer for two hours, washed in buffer, dehydrated in an increasing acetone series and embedded in EMBed 812 epoxy resin. After polymerisation for 48 hours at 60°C, embryos were cut serially with an Autocut 5020 (Reichert, Austria) and a Diatome Butler knife (Diatome, Switzerland). 2 µm thick serial sections were stained according to Richardson (Richardson et al., 1960) for 10 minutes, washed, and mounted in cedarwood oil. Images were taken with a Leica DM5000B microscope using a Leica DFC 490 digital camera and Leica application suite v. 4.8 (Leica, Germany).

Electron microscopy

Embryos were fixed with 2.5% glutaraldehyde in 0.01M sodium cacodylate buffer containing 5% sucrose at 4°C for two hours. After washing in cacodylate buffer, specimens were post fixed in reduced osmium (2% osmium tetroxide and 3% potassium ferrocyanide in 0.1M cacodylate buffer) for two hours at 4°C, dehydrated in an ethanol series, critical point dried with an EMS 850 CPD (Electron Microscopy Services, Germany), mounted and 20 nm gold sputtered with a CCU-010 sputter coater (Safematic, Switzerland), and examined with a DSM950 scanning electron microscope (Zeiss, Germany). Images were taken with a Pentax digital camera and PK_Tether 0.7.0 free software.

Data Presentation and Analysis

All data presented in this study were analyzed with R using the RStudio integrated development environment and plotted using the “ggplot2” package (Rstudio Team, 2016; Wickham, 2016).

Statistical significance of differences in expression levels between groups were calculated on at least three biological replicates with the Wilcoxon rank sum test, corrected for multiple comparisons using the Benjamini-Hochberg FDR method.

Statistical significance of a difference in MP or SSF numbers between groups was determined using one-way ANOVA corrected for unequal variances and the Games-Howell post-hoc test for pairwise comparison as implemented in the "userfriendlyscience" package (Peters, 2017). P values are indicated as follows: * $p<0.05$; ** $p<0.01$; $p<0.001$; ns not significant. Sample sizes (N) are given in the respective figure legends.

Acknowledgements

We are grateful to Dzenana Tufegdzic for fish care, and to Dirk Meyer, Robin Kimmel and Kathi Klee for helpful discussions and/or comments on the manuscript. This work was supported by funding from the Austrian Science Fund (FWF) and the Tyrolean Science Fund (TWF) (FWF P27338 (to P.A.), FWF P30441 (to E.S.), TWF 236277 (to D.R.)).

Competing interests

The authors declare they have no competing interests.

References

Ayers KL, Thérond PP. 2010. Evaluating Smoothened as a G-protein-coupled receptor for Hedgehog signalling. *Trends Cell Biol* **20**:287–298. doi:10.1016/j.tcb.2010.02.002

Bachmann VA, Mayrhofer JE, Ilouz R, Tschaikner P, Raffeiner P, Röck R, Courcelles M, Apelt F, Lu T-W, Baillie GS, Thibault P, Aanstad P, Stelzl U, Taylor SS, Stefan E. 2016. Gpr161 anchoring of PKA consolidates GPCR and cAMP signaling. *Proc Natl Acad Sci* **113**:7786–7791. doi:10.1073/pnas.1608061113

Barresi MJ, Stickney HL, Devoto SH. 2000. The zebrafish slow-muscle-omitted gene product is required for Hedgehog signal transduction and the development of slow muscle identity. *Development* **127**:2189–2199.

Barth KA, Wilson SW. 1995. Expression of zebrafish nk2.2 is influenced by sonic hedgehog/vertebrate hedgehog-1 and demarcates a zone of neuronal differentiation in the embryonic forebrain. *Development* **121**:1755–1768.

Briscoe J, Sussel L, Serup P, Hartigan-O'Connor D, Jessell TM, Rubenstein JLR, Ericson J. 1999. Homeobox gene Nkx2.2 and specification of neuronal identity by graded Sonic hedgehog signalling. *Nature* **398**:622–627. doi:10.1038/19315

Briscoe J, Thérond PP. 2013. The mechanisms of Hedgehog signalling and its roles in development and disease. *Nat Rev Mol Cell Biol* **14**:416–429.

Carr AC, Moore SD. 2012. Robust Quantification of Polymerase Chain Reactions Using Global Fitting.

PLoS One **7**:e37640. doi:10.1371/journal.pone.0037640

Chen W, Burgess S, Hopkins N. 2001. Analysis of the zebrafish smoothened mutant reveals conserved and divergent functions of hedgehog activity. *Development* **128**:2385–2396.

Chung W-S, Stainier DYR. 2008. Intra-Endodermal Interactions Are Required for Pancreatic β Cell Induction. *Dev Cell* **14**:582–593. doi:10.1016/j.devcel.2008.02.012

Concordet JP, Lewis KE, Moore JW, Goodrich L V, Johnson RL, Scott MP, Ingham PW. 1996. Spatial regulation of a zebrafish patched homologue reflects the roles of sonic hedgehog and protein kinase A in neural tube and somite patterning. *Development* **122**:2835–46.

Corbit KC, Aanstad P, Singla V, Norman AR, Stainier DYR, Reiter JF. 2005. Vertebrate Smoothened functions at the primary cilium. *Nature* **437**:1018–1021. doi:10.1038/nature04117

Dessaud E, Yang LL, Hill K, Cox B, Ulloa F, Ribeiro A, Mynett A, Novitch BG, Briscoe J. 2007. Interpretation of the sonic hedgehog morphogen gradient by a temporal adaptation mechanism. *Nature* **450**:717–720. doi:10.1038/nature06347

Edgar RC. 2004. MUSCLE: multiple sequence alignment with high accuracy and high throughput. *Nucleic Acids Res* **32**:1792–1797. doi:10.1093/nar/gkh340

García-Nafría J, Watson JF, Greger IH. 2016. IVA cloning: A single-tube universal cloning system exploiting bacterial In Vivo Assembly. *Sci Rep* **6**:27459. doi:10.1038/srep27459

Guner B, Karlstrom RO. 2007. Cloning of zebrafish nkx6.2 and a comprehensive analysis of the conserved transcriptional response to Hedgehog/Gli signaling in the zebrafish neural tube. *Gene Expr Patterns* **7**:596–605. doi:10.1016/j.modgep.2007.01.002

Hammerschmidt M, Bitgood MJ, McMahon AP. 1996. Protein kinase A is a common negative regulator of Hedgehog signaling in the vertebrate embryo. *Genes Dev* **10**:647–658. doi:10.1101/gad.10.6.647

Huang P, Ahkmetova L, Schier AF, Zimmerman S, Pauli A, Thyme SB, Gagnon JA, Montague TG, Richter C, Valen E. 2014. Efficient mutagenesis by Cas9 protein-mediated oligonucleotide insertion and large-scale assessment of single-guide RNAs. *PLoS One* **9**:e98186. doi:10.1371/journal.pone.0098186

Hui C-C, Angers S. 2011. Gli proteins in development and disease. *Annu Rev Cell Dev Biol* **27**:513–537. doi:10.1146/annurev-cellbio-092910-154048

Humke EW, Dorn K V, Milenkovic L, Scott MP, Rohatgi R. 2010. The output of Hedgehog signaling is controlled by the dynamic association between Suppressor of Fused and the Gli proteins. *Genes*

448 *Dev* **24**:670–682. doi:10.1101/gad.1902910

449 Hwang S-H, White KA, Somatilaka BN, Shelton JM, Richardson JA, Mukhopadhyay S. 2018. The G
450 protein-coupled receptor Gpr161 regulates forelimb formation, limb patterning and skeletal
451 morphogenesis in a primary cilium-dependent manner. *Development* **145**:dev154054.
452 doi:10.1242/dev.154054

453 Ingham PW, Nakano Y, Seger C. 2011. Mechanisms and functions of Hedgehog signalling across the
454 metazoa. *Nat Rev Genet* **12**:393–406.

455 Jiang J, Hui C. 2008. Hedgehog Signaling in Development and Cancer. *Dev Cell* **15**:801–812.
456 doi:10.1016/j.devcel.2008.11.010

457 Kimmel CB, Ballard WW, Kimmel SR, Ullmann B, Schilling TF. 1995. Stages of embryonic development
458 of the zebrafish. *Dev Dyn* **203**:253–310. doi:10.1002/aja.1002030302

459 Klein RS, Rubin JB, Gibson HD, DeHaan EN, Alvarez-Hernandez X, Segal RA, Luster AD. 2001. SDF-1
460 alpha induces chemotaxis and enhances Sonic hedgehog-induced proliferation of cerebellar
461 granule cells. *Development* **128**:1971–81.

462 Koudijs MJ, den Broeder MJ, Groot E, van Eeden FJ. 2008. Genetic analysis of the two zebrafish
463 patched homologues identifies novel roles for the hedgehog signaling pathway. *BMC Dev Biol*
464 **8**:15. doi:10.1186/1471-213X-8-15

465 Koudijs MJ, den Broeder MJ, Keijser A, Wienholds E, Houwing S, van Rooijen EMHC, Geisler R, van
466 Eeden FJM. 2005. The Zebrafish Mutants dre, uki, and lep Encode Negative Regulators of the
467 Hedgehog Signaling Pathway. *PLoS Genet* **1**:e19. doi:10.1371/journal.pgen.0010019

468 Krauss S, Concordet J-P, Ingham PW. 1993. A functionally conserved homolog of the Drosophila
469 segment polarity gene hh is expressed in tissues with polarizing activity in zebrafish embryos.
470 *Cell* **75**:1431–1444. doi:10.1016/0092-8674(93)90628-4

471 Li BI, Matteson PG, Ababon MF, Nato AQ, Lin Y, Nanda V, Matise TC, Millonig JH. 2015. The orphan
472 GPCR, Gpr161, regulates the retinoic acid and canonical Wnt pathways during neurulation. *Dev*
473 *Biol* **402**:17–31. doi:10.1016/j.ydbio.2015.02.007

474 Marks SA, Kalderon D. 2011. Regulation of mammalian Gli proteins by Costal 2 and PKA in Drosophila
475 reveals Hedgehog pathway conservation. *Development* **138**:2533–2542.
476 doi:10.1242/dev.063479

477 Montague TG, Cruz JM, Gagnon JA, Church GM, Valen E. 2014. CHOPCHOP: a CRISPR/Cas9 and TALEN
478 web tool for genome editing. *Nucleic Acids Res* **42**:W401–W407. doi:10.1093/nar/gku410

479 Mukhopadhyay S, Wen X, Ratti N, Loktev A, Rangell L, Scales SJ, Jackson PK. 2013. The ciliary G-
480 protein-coupled receptor Gpr161 negatively regulates the Sonic hedgehog pathway via cAMP
481 signaling. *Cell* **152**:210–223. doi:10.1016/j.cell.2012.12.026

482 Niewiadomski P, Kong JH, Ahrends R, Ma Y, Humke EW, Khan S, Teruel MN, Novitch BG, Rohatgi R.
483 2014. Gli Protein Activity Is Controlled by Multisite Phosphorylation in Vertebrate Hedgehog
484 Signaling. *Cell Rep* **6**:168–181. doi:10.1016/j.celrep.2013.12.003

485 Niewiadomski P, Niedziółka SM, Markiewicz Ł, Uśpieński T, Baran B, Chojnowska K. 2019. Gli
486 Proteins: Regulation in Development and Cancer. *Cells* **8**:147. doi:10.3390/cells8020147

487 Nørholm MH. 2010. A mutant Pfu DNA polymerase designed for advanced uracil-excision DNA
488 engineering. *BMC Biotechnol* **10**:21. doi:10.1186/1472-6750-10-21

489 Ogden SK, Fei DL, Schilling NS, Ahmed YF, Hwa J, Robbins DJ. 2008. G protein Gαi functions
490 immediately downstream of Smoothened in Hedgehog signalling. *Nature* **456**:967–970.
491 doi:10.1038/nature07459

492 Pal K, Hwang S, Somatilaka B, Badgandi H, Jackson PK, DeFea K, Mukhopadhyay S. 2016. Smoothened
493 determines β-arrestin–mediated removal of the G protein–coupled receptor Gpr161 from the
494 primary cilium. *J Cell Biol* **212**:861–875. doi:10.1083/jcb.201506132

495 Pan Y, Wang C, Wang B. 2009. Phosphorylation of Gli2 by protein kinase A is required for Gli2
496 processing and degradation and the Sonic Hedgehog-regulated mouse development. *Dev Biol*
497 **326**:177–189. doi:10.1016/j.ydbio.2008.11.009

498 Park H-C, Mehta A, Richardson JS, Appel B. 2002. olig2 Is Required for Zebrafish Primary Motor
499 Neuron and Oligodendrocyte Development. *Dev Biol* **248**:356–368.
500 doi:10.1006/DBIO.2002.0738

501 Peters G-JY. 2017. userfriendlyscience: Quantitative analysis made accessible. *R Packag version 06-1*.
502 doi:10.17605/OSF.IO/TXEQU

503 Pusapati G V., Kong JH, Patel BB, Gouti M, Sagner A, Sircar R, Luchetti G, Ingham PW, Briscoe J,
504 Rohatgi R. 2018. G protein-coupled receptors control the sensitivity of cells to the morphogen
505 Sonic Hedgehog. *Sci Signal* **11**:1–16. doi:10.1126/scisignal.aao5749

506 Raleigh DR, Reiter JF. 2019. Misactivation of Hedgehog signaling causes inherited and sporadic
507 cancers. *J Clin Invest*. doi:10.1172/JCI120850

508 Regard JB, Malhotra D, Gvozdenovic-Jeremic J, Josey M, Chen M, Weinstein LS, Lu J, Shore EM,
509 Kaplan FS, Yang Y. 2013. Activation of Hedgehog signaling by loss of GNAS causes heterotopic

ossification. *Nat Med* **19**:1505–12. doi:10.1038/nm.3314

Richardson KC, Jarett L, Finke EH. 1960. Embedding in epoxy resins for ultrathin sectioning in electron microscopy. *Biotech Histochem* **35**:313–323. doi:10.3109/10520296009114754

Riobo NA, Saucy B, DiLizio C, Manning DR. 2006. Activation of heterotrimeric G proteins by Smoothened. *Proc Natl Acad Sci* **103**:12607–12612. doi:10.1073/pnas.0600880103

Ritz C, Spiess A-N. 2008. qpcR: an R package for sigmoidal model selection in quantitative real-time polymerase chain reaction analysis. *Bioinformatics* **24**:1549–1551. doi:10.1093/bioinformatics/btn227

Rödiger S, Burdukiewicz M, Spiess A-N, Blagodatskikh K. 2017. Enabling reproducible real-time quantitative PCR research: the RDML package. *Bioinformatics* **33**:4012–4014. doi:10.1093/bioinformatics/btx528

Rstudio Team. 2016. RStudio: Integrated development for R. RStudio, Inc., Boston MA. *RStudio*.

Schmitt EA, Dowling JE. 1999. Early retinal development in the zebrafish, Danio rerio: Light and electron microscopic analyses. *J Comp Neurol* **404**:515–536. doi:10.1002/(SICI)1096-9861(19990222)404:4<515::AID-CNE8>3.0.CO;2-A

Shimada IS, Hwang S-HH, Somatilaka BN, Wang X, Skowron P, Kim J, Kim M, Shelton JM, Rajaram V, Xuan Z, Taylor MD, Mukhopadhyay S. 2018. Basal Suppression of the Sonic Hedgehog Pathway by the G-Protein-Coupled Receptor Gpr161 Restricts Medulloblastoma Pathogenesis. *Cell Rep* **22**:1169–1184. doi:10.1016/j.celrep.2018.01.018

Singh J, Wen X, Scales SJ. 2015. The orphan G protein-coupled receptor Gpr175 (Tpra40) enhances Hedgehog signaling by modulating cAMP levels. *J Biol Chem*. doi:10.1074/jbc.M115.665810

Stückemann T, Wegleiter T, Stefan E, Nägele O, Tarbashevich K, Böck G, Raz E, Aanstad P. 2012. Zebrafish Cxcr4a determines the proliferative response to Hedgehog signalling. *Development* **139**:2711–2720.

Torres-Quesada O, Mayrhofer JE, Stefan E. 2017. The many faces of compartmentalized PKA signalosomes. *Cell Signal* **37**:1–11. doi:10.1016/j.cellsig.2017.05.012

Tuson M, He MM, Anderson K V. 2011. Protein kinase A acts at the basal body of the primary cilium to prevent Gli2 activation and ventralization of the mouse neural tube. *Development* **138**:4921–4930. doi:10.1242/dev.070805

Wang B, Fallon JF, Beachy PA. 2000. Hedgehog-Regulated Processing of Gli3 Produces an Anterior/Posterior Repressor Gradient in the Developing Vertebrate Limb. *Cell* **100**:423–434.

doi:10.1016/S0092-8674(00)80678-9

Whitfield TT, Granato M, van Eeden FJ, Schach U, Brand M, Furutani-Seiki M, Haffter P, Hammerschmidt M, Heisenberg CP, Jiang YJ, Kane DA, Kelsh RN, Mullins MC, Odenthal J, Nüsslein-Volhard C. 1996. Mutations affecting development of the zebrafish inner ear and lateral line. *Development* **123**:241–54. doi:10.1016/S1350-9462(98)00010-X

Wickham H. 2016. ggplot2: Elegant Graphics for Data Analysis, Use R! Springer-Verlag New York. doi:10.1007/978-3-319-24277-4

Wolff C, Roy S, Ingham PW. 2003. Multiple muscle cell identities induced by distinct levels and timing of Hedgehog activity in the zebrafish embryo. *Curr Biol* **13**:1169–1181. doi:10.1016/S0960-9822(03)00461-5

Zhao Z, Lee RTH, Pusapati G V, Iyu A, Rohatgi R, Ingham PW. 2016. An essential role for Grk2 in Hedgehog signalling downstream of Smoothened. *EMBO Rep* **17**:739–752. doi:10.15252/embr.201541532

Figures

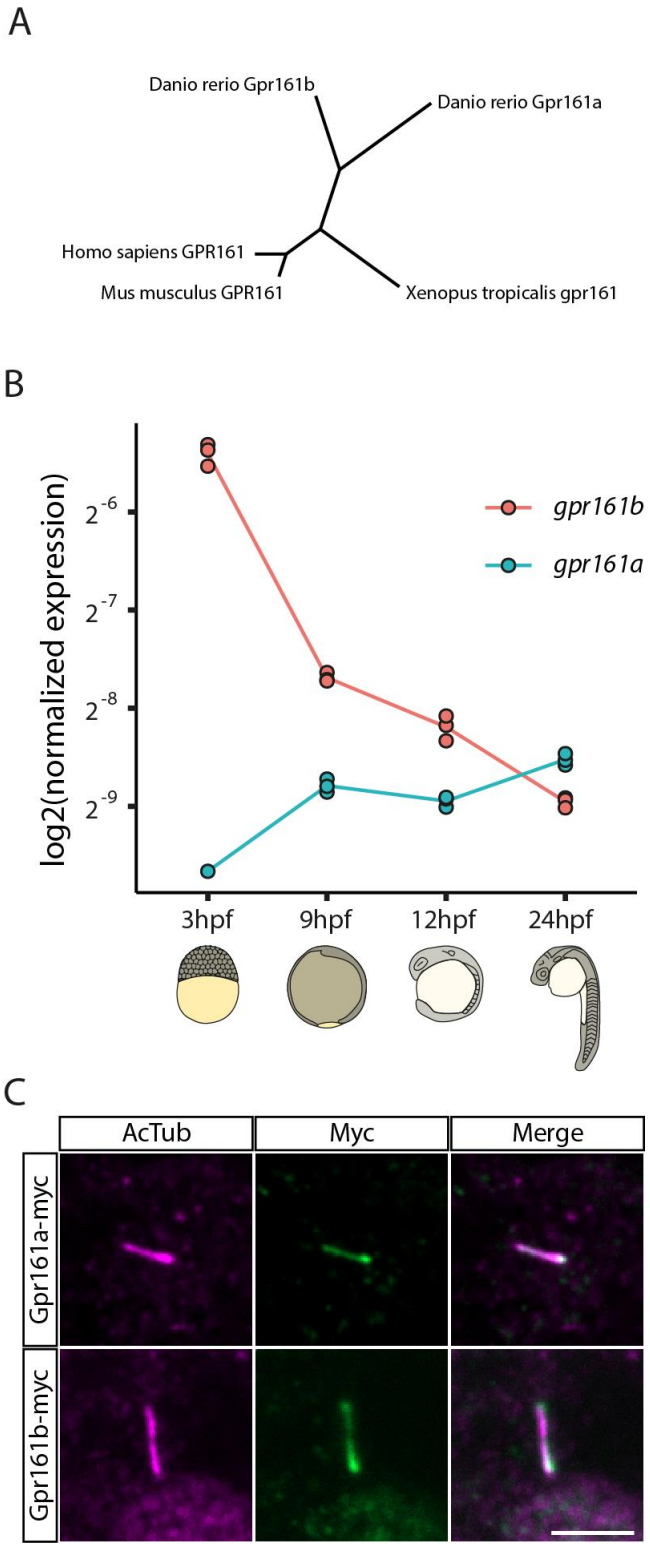

Figure 1. Gpr161 is a conserved ciliary GPCR. (A) Un-rooted cladogram showing the relation between Gpr161 protein sequences of selected organisms. **(B)** *gpr161a* and *gpr161b* transcript levels at different stages of development analysed in whole embryo lysates in triplicates using RT-qPCR. **(C)** Wildtype embryos were injected with *gpr161a-myc* or *gpr161b-myc* mRNA at one-cell stage and fixed at 9 hpf before immunostaining for acetylated tubulin (AcTub; purple), a marker for the ciliary axoneme and Myc (green) (scale bar: 5µm).

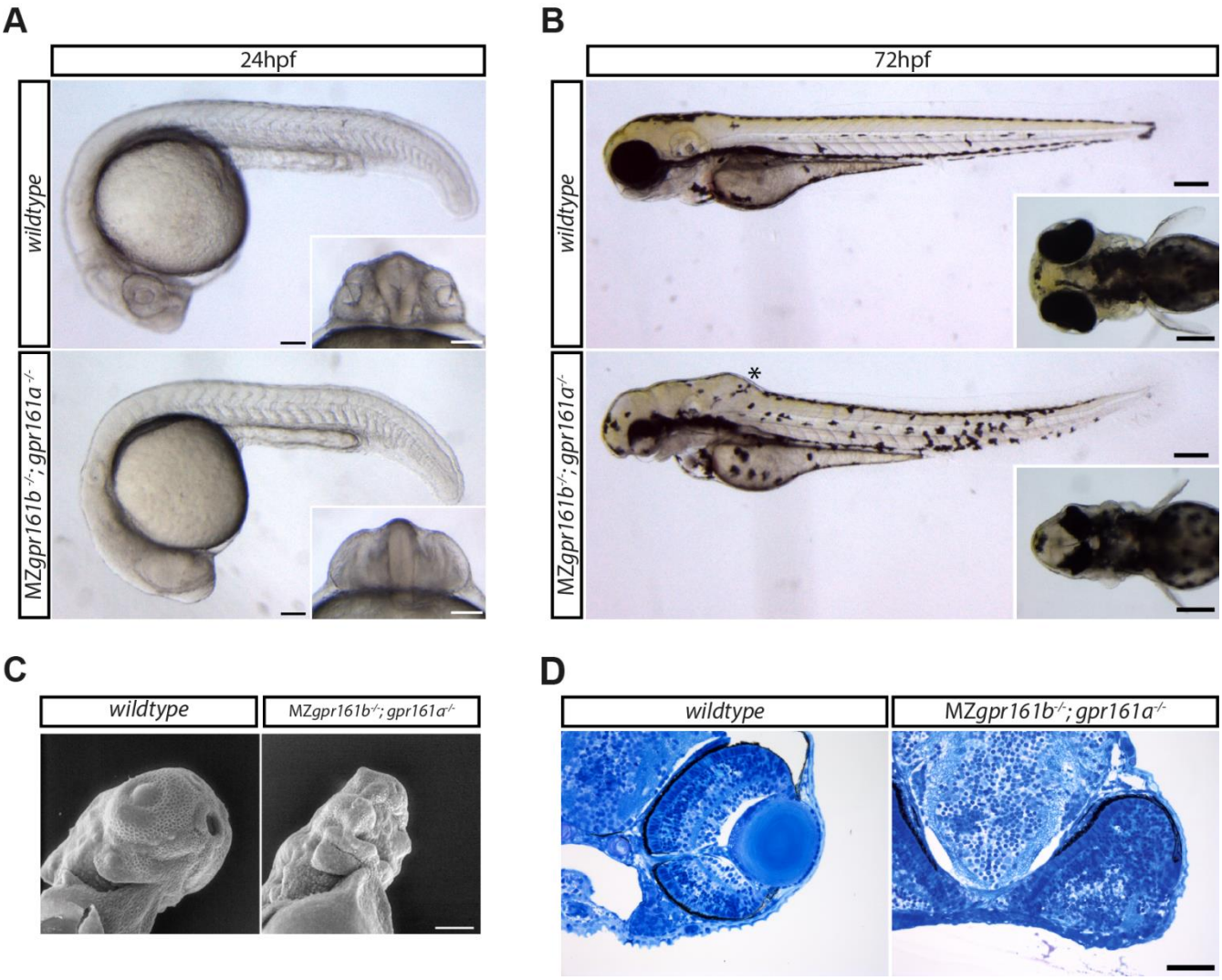

Figure 2. Gpr161 is essential during embryonic development. (A) Lateral view of wildtype and MZ*gpr161b*$^{-/-}$*; gpr161a*$^{-/-}$ embryos at 24 hpf (scale bars: 100µm); Insets: ventral view of the developing eyes. **(B)** Wildtype and MZ*gpr161b*$^{-/-}$*; gpr161a*$^{-/-}$ embryos at 72 hpf; Asterisk indicates swollen hindbrain (scale bars: 200µm); Insets: dorsal view of the head **(C)** Ventrolateral-view of the craniofacial region of wildtype and MZ*gpr161b*$^{-/-}$*; gpr161a*$^{-/-}$ embryos at 72 hpf taken by scanning electron microscopy (scale bar: 100µm). **(D)** Transverse semi-thin sections of the eye in wildtype and MZ*gpr161b*$^{-/-}$*; gpr161a*$^{-/-}$ embryos fixed at 72 hpf (Richardson staining, scale bars: 50µm).

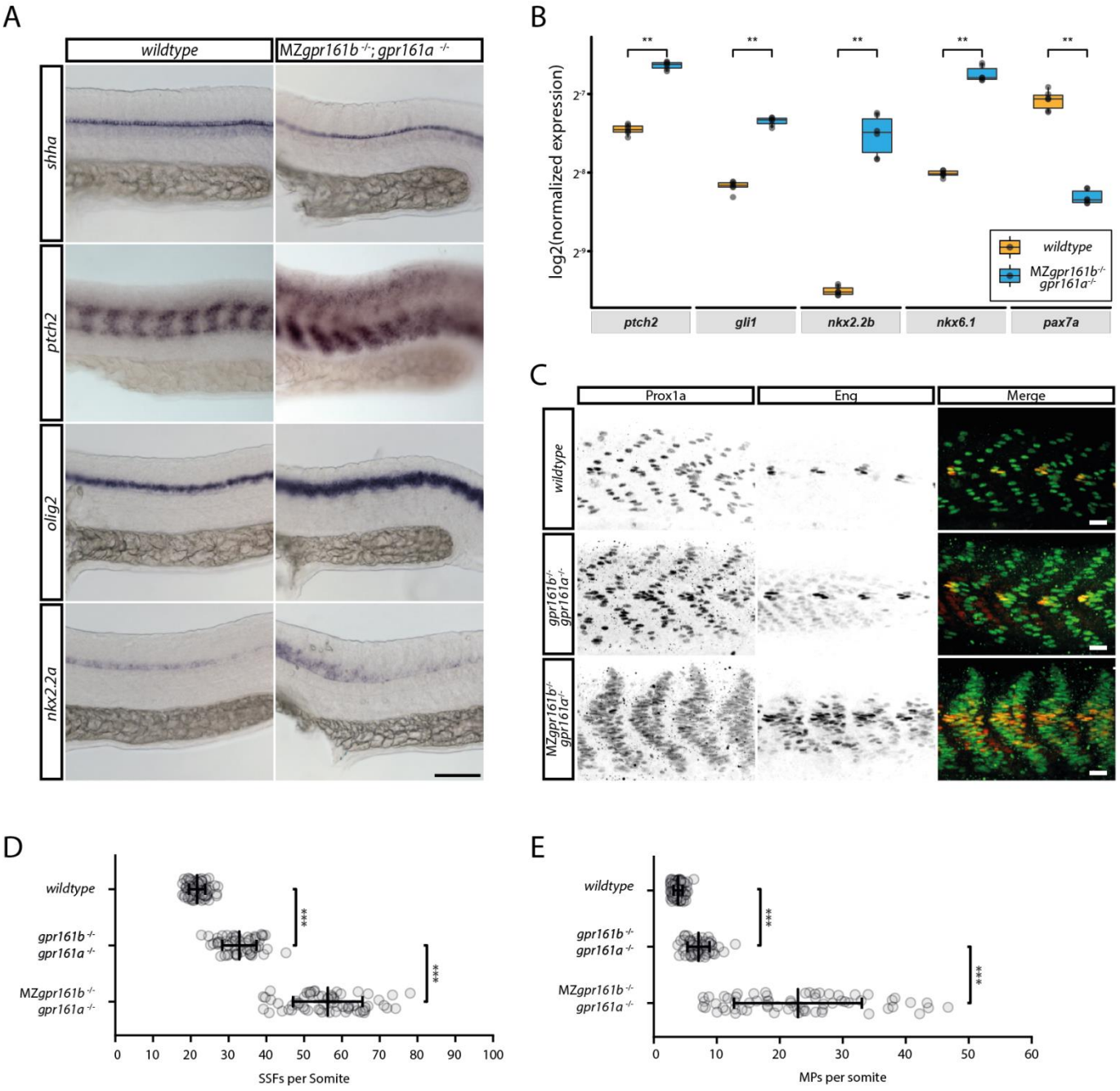

Figure 3. Hh signalling activity is increased in *gpr161* mutants. (A) RNA in situ hybridization of *shh, ptch2, olig2* and *nkx2.2a* transcripts in wildtype and MZ*gpr161b* $^{-/-}$*; gpr161a* $^{-/-}$ embryos fixed at 24 hpf (lateral view, scale bar: 100µm). **(B)** Transcript levels of *ptch2, gli1, nkx2.2b, nkx6.1* and *pax7a* in wildtype and MZ*gpr161b* $^{-/-}$*; gpr161a* $^{-/-}$ embryos at 24hpf determined by RT-qPCR (n=3)**(C)** Immunostaining of Prox1 and Eng proteins in 24 hpf zebrafish embryos reveal the number of MPs (Prox1a/Eng double positive) as well as SFFs (Prox1 positive) in wild-type, *gpr161b*$^{-/-}$*; gpr161a*$^{-/-}$ and MZ*gpr161b* $^{-/-}$*; gpr161* $^{-/-}$ embryos fixed at 24 hpf (scale bar: 20µm). Number of **(D)** SSFs and **(E)** MPs per somite in wild-type (n= 93 somites in 22 embryos), *gpr161b*$^{-/-}$*; gpr161a*$^{-/-}$ (n=60 somites in 20 embryos) and MZ*gpr161b* $^{-/-}$*; gpr161a* $^{-/-}$ (n= 66 somites in 22 embryos) embryos fixed at 24 hpf.

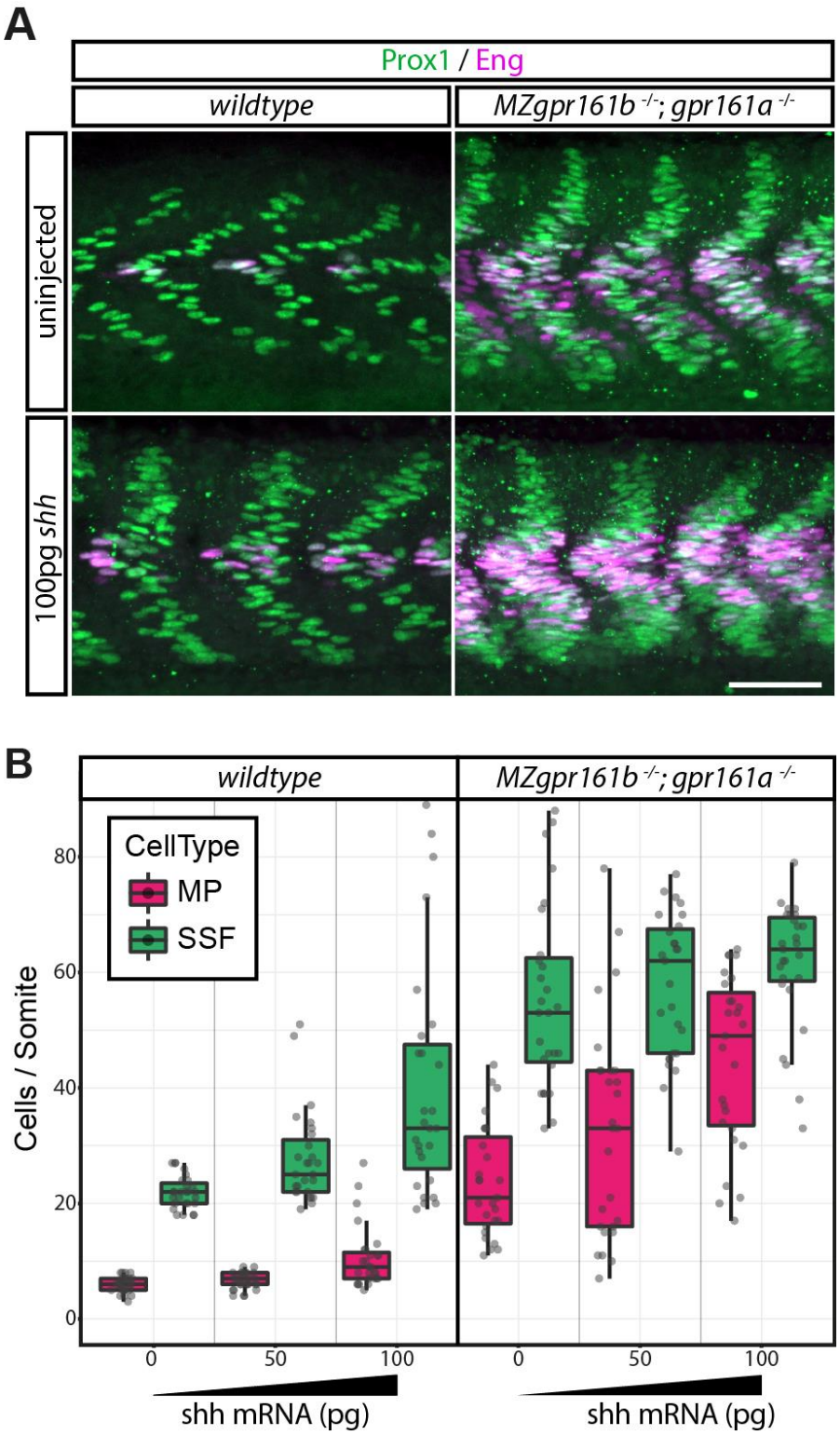

Figure 4. Injection of *shh* mRNA can elevate hh signalling outcomes in gpr161 mutants. (A) Prox1 (green)/ Eng (purple) immunostainings of wild-type and MZ*gpr161b*$^{-/-}$*; gpr161a*$^{-/-}$ embryos injected with 100 pg of *shha* mRNA (scale bar: 50µm). **(B)** Quantification of MPs and SSFs in wild-type and MZ*gpr161b*$^{-/-}$*; gpr161a*$^{-/-}$ embryos injected with increasing amounts of *shh* mRNA (for all experiments: n=27 somites in 9 embryos).

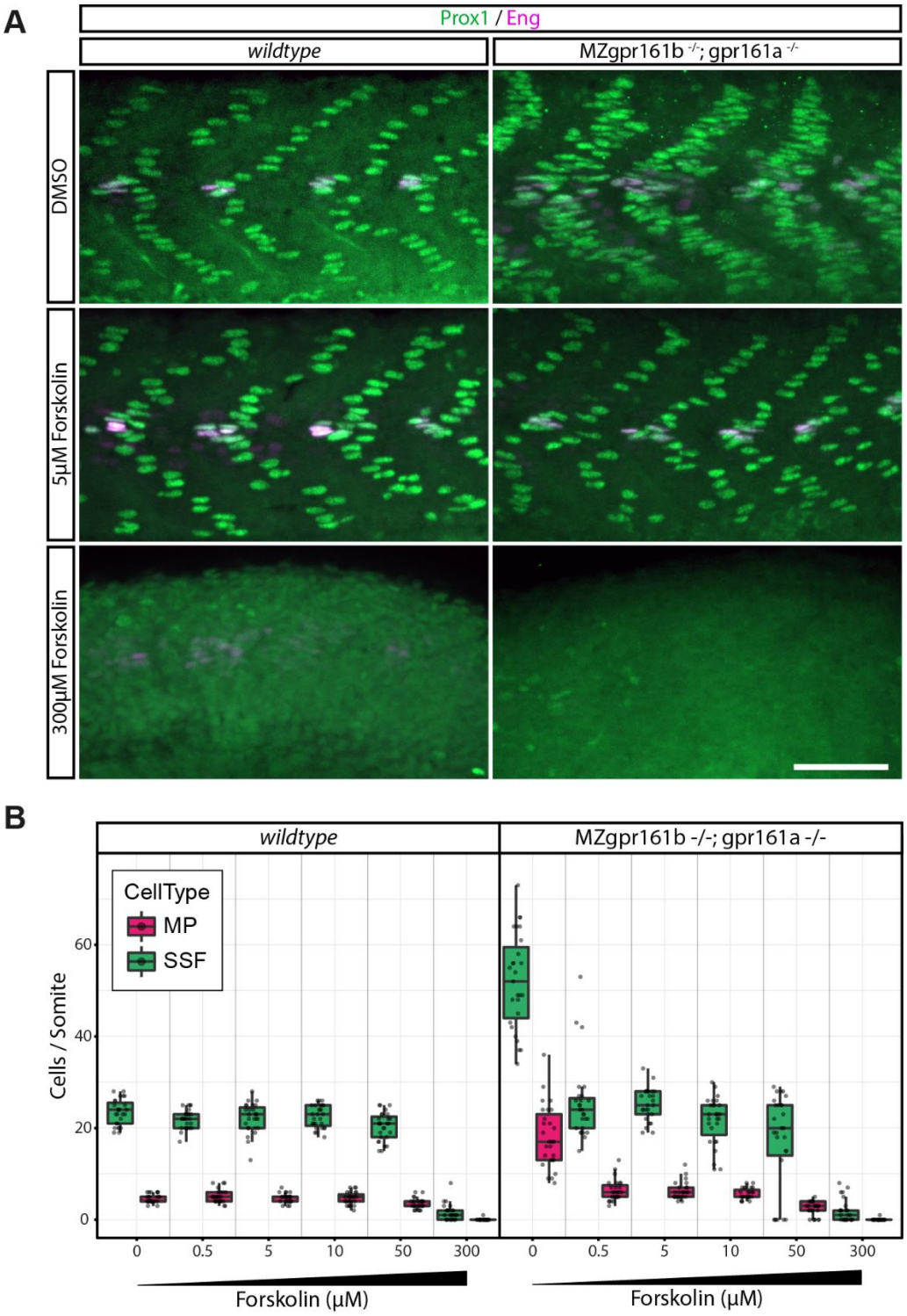

Figure 5. Forskolin treatments can rescue the gpr161 phenotype. (A) Prox1 (green)/ Eng (purple) immunostainings of wild-type and MZ*gpr161b*$^{-/-}$*; gpr161a*$^{-/-}$ embryos treated with increasing concentrations of forskolin (scale bar: 50µm). **(B)** Quantification of MPs and SSFs in wild-type and MZ*gpr161b*$^{-/-}$*; gpr161a*$^{-/-}$ embryos treated with increasing concentrations of forskolin (for each experiment, n=27 somites in 9 embryos).

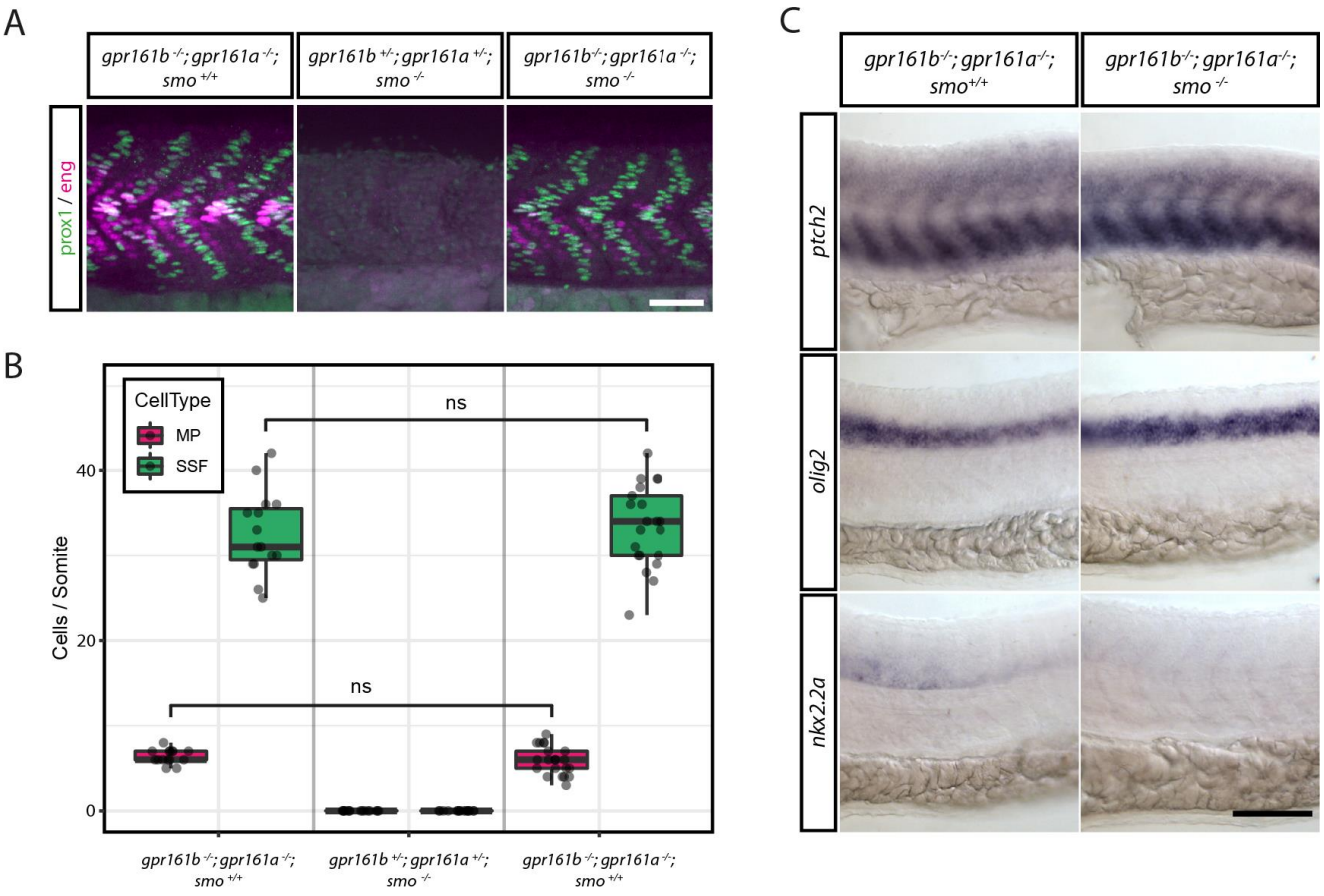

Figure 6. The requirement for Smo during high-level Hh signalling in *gpr161* mutants is tissue-specific. (A) Prox1 (green)/ Eng (purple) immunostainings of wildtype and MZgpr161b$^{-/-}$; gpr161a$^{-/-}$ embryos at 24 hpf after DMSO or 200µM Cyclopamine treatment (scale bar: 50µm). **(B)** Quantification of MPs and SSFs from experiment presented in A (*gpr161b$^{-/-}$; gpr161a$^{-/-}$; smo$^{+/+}$* and *gpr161b$^{+/-}$; gpr161a$^{+/-}$; smo$^{-/-}$*: n=15 somites in 5 embryos; *gpr161b$^{-/-}$; gpr161a$^{-/-}$; smo$^{-/-}$*: n=21 somites in 7 embryos; all others: n=27 somites in 9 embryos). **(C)** RNA in situ hybridization of *ptch2, olig2* and *nkx2.2a* transcripts in *gpr161b$^{-/-}$; gpr161a$^{-/-}$; smo$^{+/+}$* and *gpr161b$^{-/-}$; gpr161a$^{-/-}$; smo$^{-/-}$*embryos fixed at 24 hpf (lateral view, scale bar: 100µm).

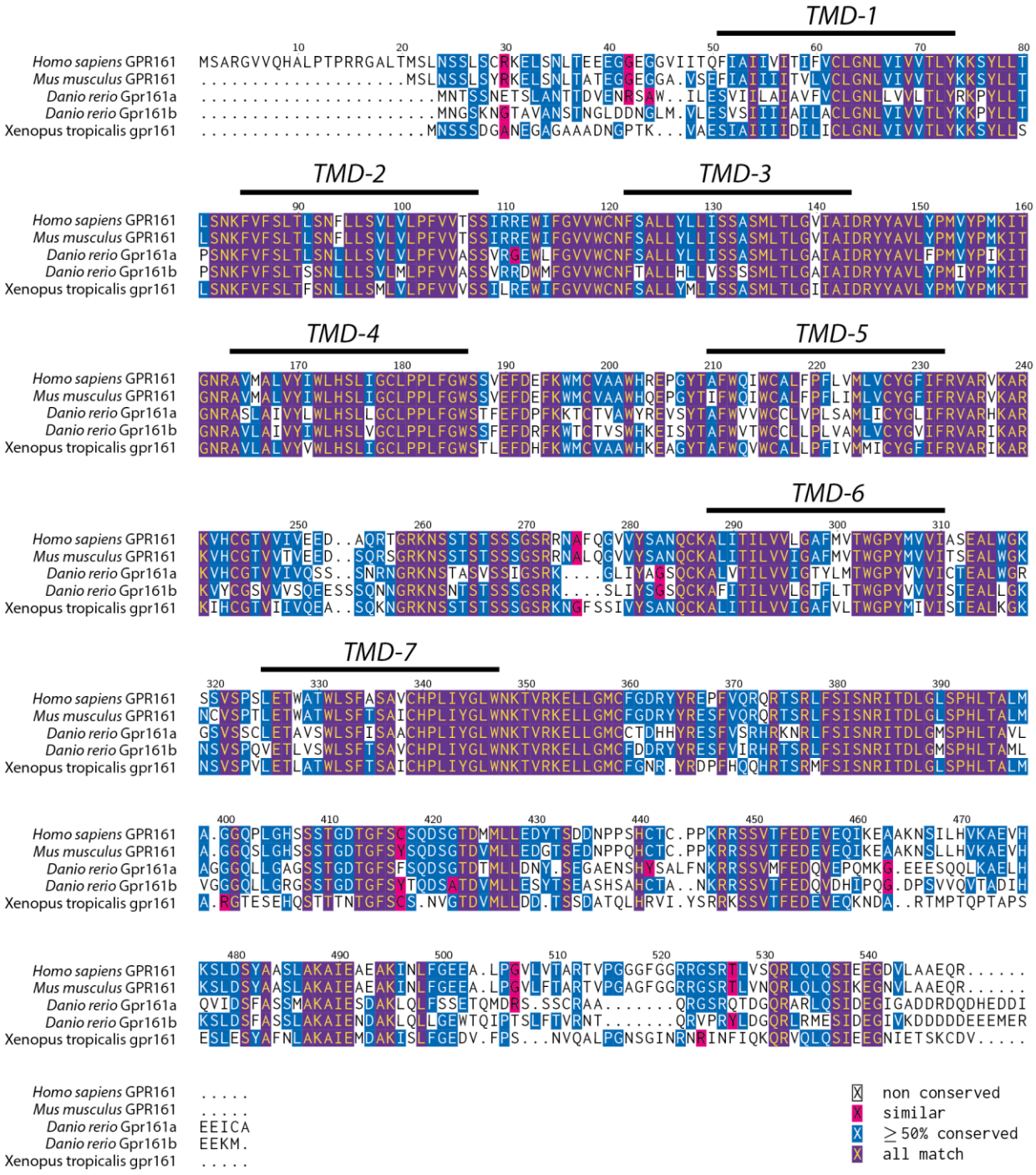

Figure 1-Supplement 1. Multiple Sequence Alignment. The sequences of the *Homo sapiens, Mus musculus, Danio rerio* and *Xenopus tropicalis* Gpr161 proteins were aligned using MUSCLE (Edgar, 2004). Transmembrane domains (TMDs) and conserved residues are indicated.

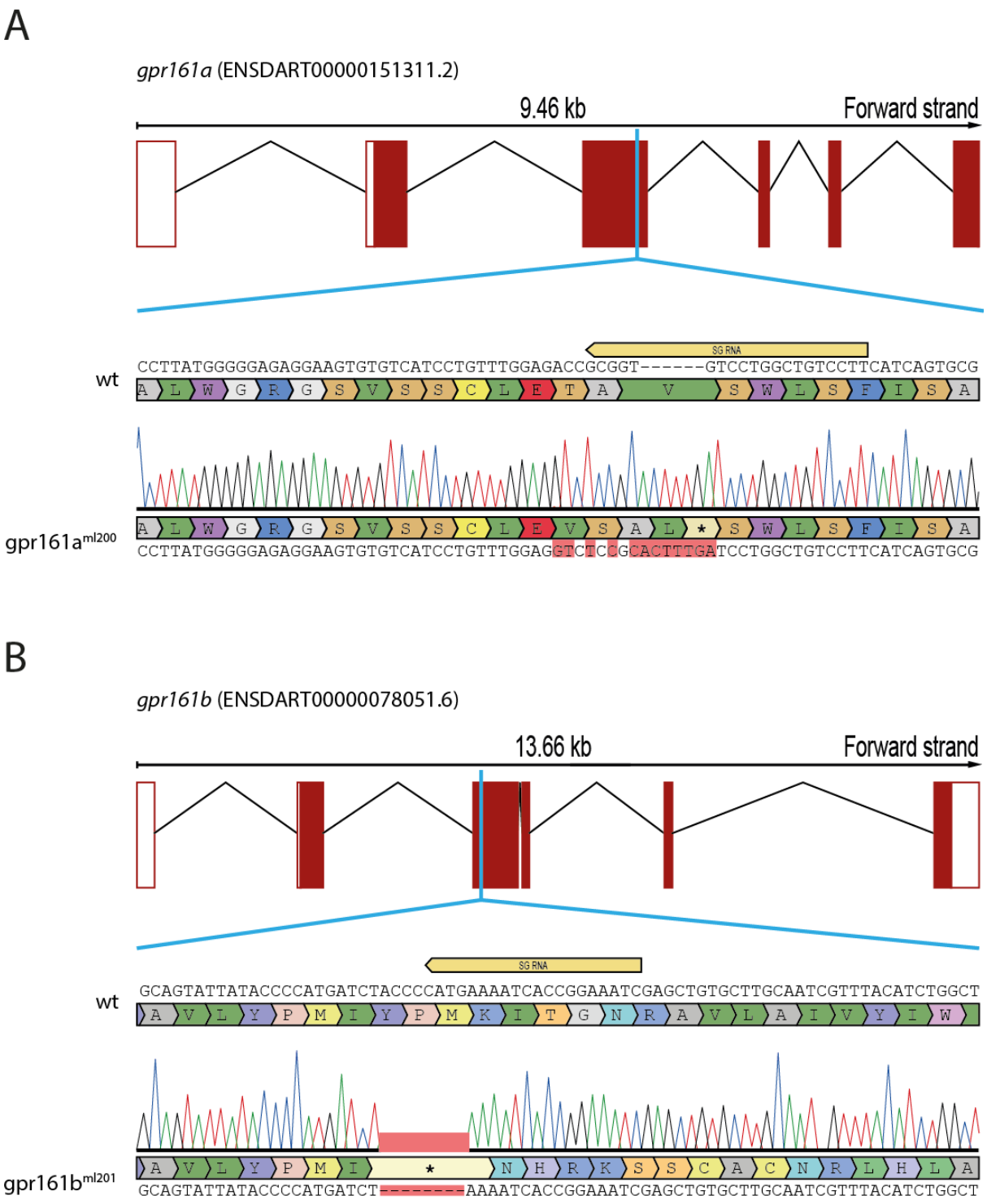

Figure 1-Supplement 2. CRISPR knock out strategy. Schematic representation of the gene structure of *gpr161a* **(A)** and *gpr161b* **(B)** indicating the position of CRISPR sgRNA recognition site and a sequence alignment of the obtained mutant alleles.

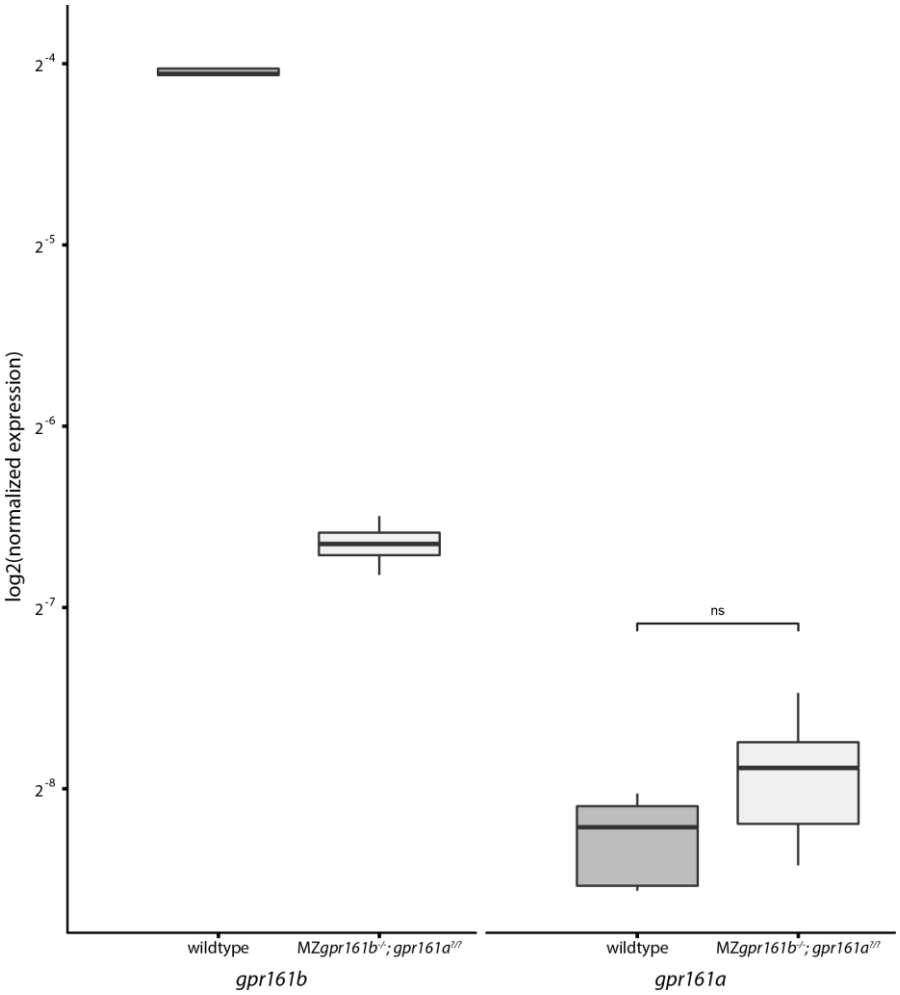

Figure 2-Supplement 1. Maternal loss of *gpr161b* does not lead to genetic compensation by *gpr161a*. Transcript levels of *gpr161a* and *gpr161b* in single embryos at 2-cell stage as determined by qPCR (n=6)

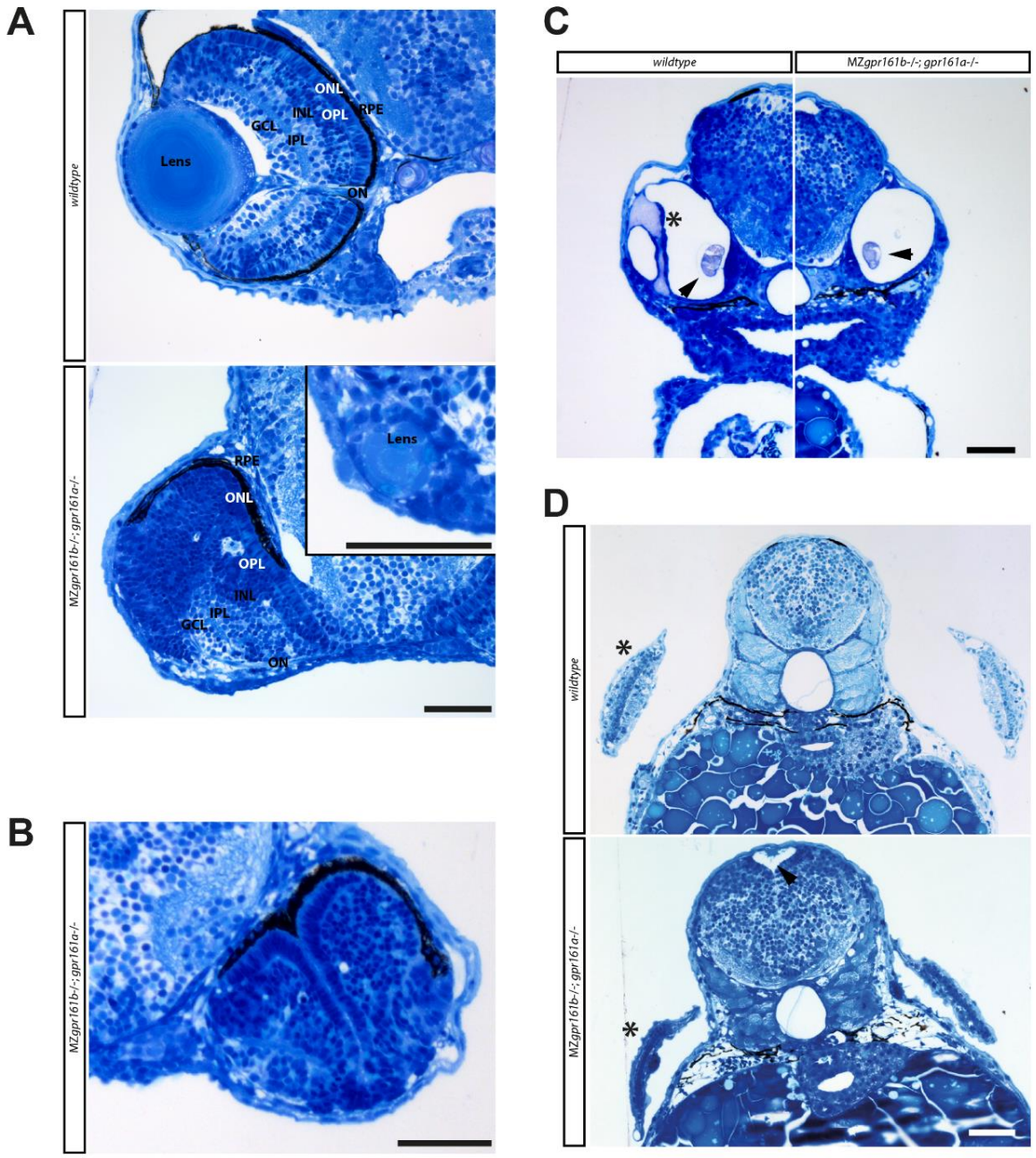

608

609 **Figure 2-Supplement 2. Severe morphological defects in *gpr161* mutant embryos at 72 hpf. (A)** Transverse section through
610 the embryonic eye at 72 hpf, Retinal layers are indicated as follows: RPE – retinal pigment epithelium, ONL – outer nuclear
611 layer, OPL - outer plexiform layer, INL – inner nuclear layer, IPL inner plexiform layer, GCL ganglion cell layer. Inset shows
612 remnant of a forming lens from a different section of the same *gpr161* mutant embryo. **(B)** Transverse section through the
613 embryonic eye of a 72 hpf *gpr161* mutant embryo shows a conspicuous invagination of the outer retinal layers. **(C)**
614 Transverse section through the otic capsule of wildtype and *gpr161* mutant embryos at 72 hpf. Asterisk highlights central
615 canal and dorsolateral septum which are missing in *gpr161* mutant embryos. Arrowhead shows otholits. **(D)** Transverse
616 section through the hindbrain region of wildtype and *gpr161* mutant embryos at 72 hpf. Asterisks highlight presence of
617 pectoral fins. Arrowhead shows enlarged brain ventricle. An increase in hindbrain diameter can be noted. (all scale bars:
618 50µm)

619

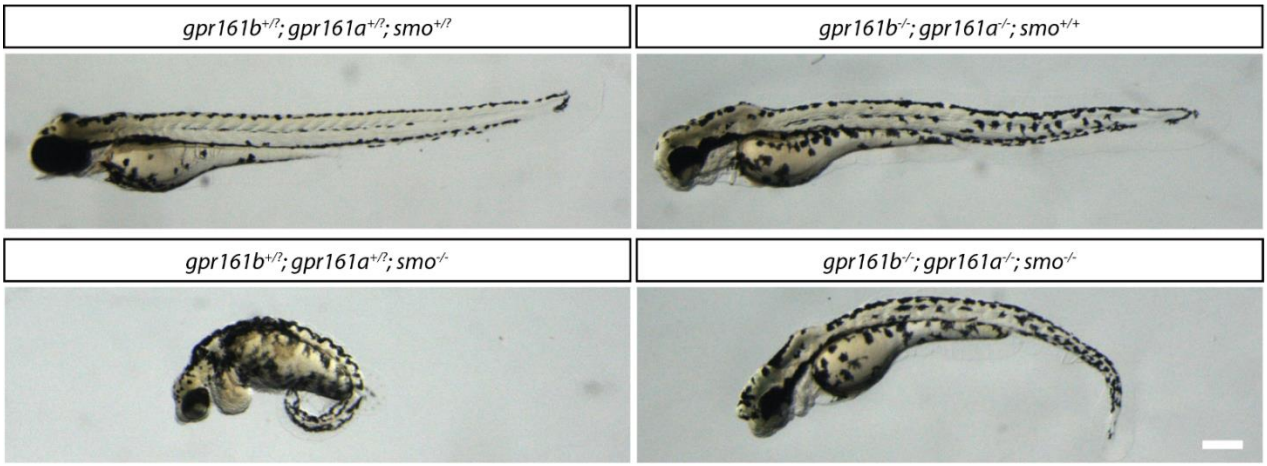

620

621 **Figure 6-Supplement 1. Morphological phenotypes of *gpr161b$^{-/-}$; gpr161a$^{-/-}$* mutants are independent of Smo.** Lateral

622 view of embryos from a gpr161b$^{+/-}$; gpr161a$^{+/-}$; smo$^{+/-}$ incross at 72hpf (scale bar: 100µm).

Tables

Table 1. List of Antibodies

Antibody	*Source*	*Dilution*	Identifier
Prox1	abcam	1:500	ab209849
Engr	DSHB	1:20	4D9
Myc	abcam	1:500	ab9106
acTub	Sigma	1:500	T7451
Alexa Fluor 647 anti mouse	ThermoFisher	1:500	A-21235
Alexa Fluor 488 anti rabbit	ThermoFisher	1:500	A-11008

Table 2. List of Primers

Name	*Used for*	*Sequence*
Gpr161a_SSLP_F	Genotyping	TGATCTGCACTGAGGCCTTATGGG
Gpr161a_SSLP_R	Genotyping	AAGAGGATGACAAGCCGCACTG
gpr161b_SSLP_F	Genotyping	CACAAGGGATTGATTGAAATG
gpr161b_SSLP_R	Genotyping	ATTGCAAGCACAGCTCGATT
gpr161a-IVA-F	Cloning	AATTCAAGGGCAAACATGAACACCAGCAGCAATGA
gpr161a-IVA-R	Cloning	CACGGAGCCACCTCCTGCGCATATTTCCTCGATAT
gpr161b-IVA-F	Cloning	AATTCAAGGGCAAACATGAACGGCTCTAAGAATGG
gpr161b-IVA-R	Cloning	CACGGAGCCACCTCCCATTTTTTCCTCGCGCTCCA
gli1_qpcr_f	qPCR	GTAAGGCCACACACACACTGATG
gli1_qpcr_r	qPCR	GCTACACCCACAGTCCTCTTTG
nkx2.2b_qpcr_f	qPCR	GTGCGGACACAAATATCCAGTGC
nkx2.2b_qpcr_r	qPCR	ATCCGCGGACAGTTCTGGATTC
nkx6.1_qpcr_f	qPCR	GACAGAGAGTCAAGTCAAGGTGTG
nkx6.1_qpcr_r	qPCR	TCCTTTCAGCCTCTCGGTTTCTG
olig2_qpcr_f	qPCR	TGCACCTGCTACCGGGAATATC
olig2_qpcr_r	qPCR	TGTCAGAGTCCATGGCGTTCAG
pax7a_qpcr_f	qPCR	ACGGCATTCTGGGAGACAAAGGTC
pax7a_qpcr_r	qPCR	TGCGTCTCTGCTTTCTCTTGAGC
eef1a1l1_qpcr_f	qPCR	TCTCTACCTACCCTCCTCTTGGTC
eef1a1l1_qpcr_r	qPCR	TTGGTCTTGGCAGCCTTCTGTG
rpl13a_qpcr_f	qPCR	ACAGGCTGAAGGTGTTTGATGGC
rpl13a_qpcr_r	qPCR	GGACAACCATGCGCTTTCTCTTG
gpr161b_qpcr_F	qPCR	ATAAGAGGAGGAGCTCGGTCAC
gpr161b_qpcr_R	qPCR	TGGACTACTGAAGGGTCACCTTG
gpr161a_qpcr_F	qPCR	AGCATCTCCAACCGAATCACAG
gpr161a_qpcr_R	qPCR	CAACATGGTGTCTGTCCCTGAG